

## FABRICATION OF REDUCED GRAPHENE OXIDE/ MOLYBDENUM DISULFIDE HETEROSTRUCTURES WITH ENHANCED FRICTION AND WEAR PERFORMANCES USED IN VACUUM ENVIRONMENT

S. ZHANG, J. DONG, L. CHEN, J. LI, C. LI\*

*Institute for Advanced Materials, School of Materials Science and Engineering, Jiangsu University, Zhenjiang, 212013, P.R. China*

Reduced graphene oxide/molybdenum disulfide (RGO/MoS<sub>2</sub>) heterostructures were fabricated by a facile and effective hydrothermal method, and the tribological properties of the heterostructures were investigated under vacuum environment. X-ray diffraction, Energy Dispersive Spectrometer, X-ray photoelectron spectrometer and Raman spectrum analysis proved that MoS<sub>2</sub> and RGO were coexisted by the chemical bonding with high purity. Scanning electron microscopy and transmission electron microscope tests show that the MoS<sub>2</sub> exhibited layer form and well dispersed on RGO nanosheets. The tribological properties of RGO/MoS<sub>2</sub> heterostructures were systematically investigated under different conditions in vacuum environment compare to pure MoS<sub>2</sub>, and the results indicated that the friction-reducing and anti-wear abilities of RGO/MoS<sub>2</sub> heterostructures were enhanced obviously. The improvement of tribological properties for RGO/MoS<sub>2</sub> heterostructures was endowed with the excellent traction and support effects of RGO nanosheets during the friction process. This work highlights a pathway to expand potential applications of MoS<sub>2</sub>, and RGO based materials in vacuum tribological field.

(Received May 26, 2017; Accepted August 5, 2017)

*Keywords:* Sulfide, RGO/MoS<sub>2</sub>, heterostructure, Tribological, Vacuum, Traction

### 1. Introduction

Regarding the space tribological studies performed growing situation, because of the development of space science and technology [1-3]. Molybdenum disulfide (MoS<sub>2</sub>), as a solid lubricant, is frequently used for space equipment's lubrication due to the crystallographic structure consisting of the covalently bonded S-Mo-S tri-layers and easy sliding between layers under the shearing force of weak van der Waals force between molecular layers [4-5]. However, one of the current challenges for MoS<sub>2</sub> is to reduce the wear and lubrication problem in vacuum environment, (1) MoS<sub>2</sub> nanosheets have poor dispersive capacity and easily agglomerated together due to the high surface areas and high chemical activity; (2) In vacuum environment, no other atoms to terminate the dangling bonds and generate the active sites, which lead to MoS<sub>2</sub> molecular structure was easy to be damaged [6-7]. These defects limit the excellent tribological properties of MoS<sub>2</sub> greatly, and reflected in the stability and wear rate of MoS<sub>2</sub> were deteriorated obviously [8]. To our knowledge, the ways to solve these problems of MoS<sub>2</sub> include modifying MoS<sub>2</sub> with other molecules or loading MoS<sub>2</sub> on support materials which have high surface areas. Efeoglu et al. obtained the MoS<sub>2</sub>-Nb nanocomposites and tested the tribological performances in vacuum environment, which show better anti-wear ability than untreated MoS<sub>2</sub> nanosheets owing to the lack of degree of freedom such as intercrystallite slippage [9]. Ding et al. tested the tribological performances of Cr- and Ti-doped MoS<sub>2</sub> in vacuum environment, and achieved the similar tribological results [10]. Although modifying MoS<sub>2</sub> with metallic molecules can enhance the anti-wear ability of MoS<sub>2</sub> in vacuum environment, they will also bring forth many problems such

---

\*Corresponding author: lichangsheng@mail.ujs.edu.cn

as high-cost, uncontrollability, and even sacrifice the lubricating ability of MoS<sub>2</sub> [11-13]. Therefore, it would be desirable to solve the agglomeration and enhance the anti-wear ability of MoS<sub>2</sub> by loading on support materials.

Graphene, a two-dimensional material composed of sp<sup>2</sup> carbon atoms arranged in a honeycomb structure, and it is an attractive ultra-thin material in lubrication engineering for reducing friction and wear [14-16]. As the result, graphene has been emerging as an ideal support for nanosheets to form hybrid materials [17-19]. Layered hybrids/heterostructures, usually obtained in the presence 2D nanomaterials, show inherent synergistic effects combining the properties of the components of the hybrid [20]. This leads to the superior performances of layered hybrids in various applications [21, 22]. Therefore, it can be reasonably inferred the heterostructures that composed of graphene and various solid lubricating nanosheets have obvious advantages than single nanomaterials in tribology. Wang et al. have researched the tribological of RGO/MoS<sub>2</sub> nanocomposites as lubricant additive in polyalkylene glycol, which shows an obvious improvement of friction-reducing ability compare to the single MoS<sub>2</sub> [23]. Yan et al. have prepared the RGO/MoS<sub>2</sub> nanocomposites, and revealed that it can improved the mechanical and tribological properties of bismaleimide composites greatly than MoS<sub>2</sub> or RGO nanosheets [24]. However, to our knowledge, only a few efforts have dealt with the tribological behavior of RGO/MoS<sub>2</sub> heterostructures in vacuum environment.

In this paper, RGO/MoS<sub>2</sub> heterostructures are synthesized through a one-step hydrothermal method, and we performed tests to clarify the tribological properties of RGO/MoS<sub>2</sub> heterostructures in epoxy resin, from the viewpoint of vacuum tribology. Epoxy resin is chosen because of its poor lubricating property, which can more clearly reflect the improvement effects of RGO/MoS<sub>2</sub>. The results of tribological tests confirm that the obtained products have obviously reduced the friction coefficient and enhanced the anti-wear ability compare to the single MoS<sub>2</sub> nanosheets. The details of synthesis, characterization, and tribological properties of the RGO/MoS<sub>2</sub> heterostructures were described herein.

## 2. Experimental

### 2.1. Synthesis of RGO/MoS<sub>2</sub> heterostructures

Graphene oxide (GO) was prepared by a modified Hummers' method [25] with the marketable graphite. 0.20g GO was added into a beaker with 20 mL distilled water under ultrasonic treatment for 1.5 h. Then, 0.50g (NH<sub>4</sub>)<sub>6</sub>Mo<sub>7</sub>O<sub>24</sub>·4H<sub>2</sub>O, 1.0g HONH<sub>3</sub>CL and 0.1g C<sub>16</sub>H<sub>33</sub>(CH<sub>3</sub>)<sub>3</sub>NBr were dissolved in 20 mL distilled water, and added into the GO solution with magnetic stirring for 0.5 h. Next, 0.45g CH<sub>2</sub>H<sub>4</sub>S were dissolved in 10 mL distilled water and added into the above solution. Finally, the solution was transferred to a Teflon-lined autoclave (100 mL) and placed in an electric oven with 200 °C for 24 h. The as-prepared product was washed with distilled water and ethanol for several times and then dried in a vacuum oven at 60 °C for 10 h. The dark powders were obtained. For comparison, RGO was prepared at the same condition without (NH<sub>4</sub>)<sub>6</sub>Mo<sub>7</sub>O<sub>24</sub>·4H<sub>2</sub>O, HONH<sub>3</sub>CL, and CH<sub>2</sub>H<sub>4</sub>S. MoS<sub>2</sub> were synthesized following the same procedure without the addition of GO.

### 2.2. Fabrication of RGO/MoS<sub>2</sub>/epoxy coatings

Steel disk (Φ 20 mm × 3 mm in size) was polished with waterproof abrasive paper and then cleaned with acetone and ethanol for 5 min via ultrasonic. RGO/MoS<sub>2</sub> heterostructures and epoxy resin (mass ratio 5:1) were dissolved in the mixed solution of acetone and ethanol (volume ratio 1:1), and then the mixture was stirred vigorously at room temperature for 10 h. Subsequently, a curing agent was added slowly and the stirring was continued for 2 h. The coating on the steel disk was prepared by air-spraying at 0.2 MP pressure of nitrogen gas and temperature of 25 °C [26]. RGO/MoS<sub>2</sub>/epoxy coatings were obtained by cured at 70 °C for 4 h. The pure epoxy, MoS<sub>2</sub>/epoxy and RGO/epoxy coatings were prepared at the same condition.

### 2.3. Friction and wear tests

The tribological performances were studied with a universal micro-tribotester in a ball-on-disk configuration. The counterpart was a steel ball with a diameter of 6 mm. The friction coefficient was investigated under the vacuum environment with the vacuum degree of  $1.0 \times 10^{-3}$  pa and the load of 10 N, meanwhile, a range of loads (5, 10, 15, 20 and 25 N) were applied to investigate wear rate of the coating. The wear rate,  $W = V/FS$ , is defined as wear volume  $V$  divided by total sliding distance  $S$  and applied load  $F$ . The wear volume was defined as  $V=AL$ , in which  $A$  was the cross-section area of wear track, and  $L$  was the distance of worn track [26]. For all tests, the sliding speed was 0.033 m/s (one motion period of forward and backward is defined as one round, and the stroke is 10 mm).

### 2.4. Characterization

X-ray diffraction (XRD) examinations were carried out using diffractometer (D8 Advance, Bruker, Germany) with Cu  $K\alpha$  radiation ( $\lambda = 0.1546$  nm) in the range of  $5-80^\circ$ . X-ray photoelectron spectroscopy (XPS) test was measured using an X-ray photoelectron spectrometer (Escalab 250Xi, ULVCA-PHI, USA) with Al  $K\alpha$  radiation. Raman spectra (Advantage 633, DeltaNu, USA) were performed on the  $\text{MoS}_2$ , RGO and RGO/ $\text{MoS}_2$  with an excitation laser of 532 nm in wavelength. Scanning electron microscopy (SEM) measurements were carried out using field emission scanning electron microscopy (JSM-7001F, JEOL, Japan) with an energy-dispersive X-ray spectrometer (EDS). Transmission electron microscope (TEM) measurements were carried out using high-resolution microscope (JEOL-2010, JEOL, Japan) instrument, operating at an accelerating voltage of 200 kV.

## 3. Results and discussion

### 3.1. Characterization of structure and morphology

As shown in Fig. 1a, the obtained RGO/ $\text{MoS}_2$  samples display five obvious XRD diffraction peaks at  $14.1^\circ$ ,  $24^\circ$ ,  $34^\circ$ ,  $43^\circ$  and  $57^\circ$ . the  $14.1^\circ$ ,  $34^\circ$  and  $57^\circ$  corresponding to the (002), (100) and (110) planes of  $\text{MoS}_2$ , the  $24^\circ$ ,  $43^\circ$  corresponding to the (002) and (103) planes of RGO, respectively. The primary peak of both appeared around  $14.06^\circ$ , corresponding to the diffraction from (002) plane of  $\text{MoS}_2$  with the layer-to-layer spacing of 0.62 nm [27]. Similar to XRD characterization, the Raman signal intensity also suggests the controllable loading of  $\text{MoS}_2$  on RGO. The two groups of characteristic phonon peaks including  $E_{2g}^1$  ( $\sim 378$   $\text{cm}^{-1}$ ) and  $A_{1g}$  ( $\sim 405$   $\text{cm}^{-1}$ ) modes for  $\text{MoS}_2$  as well as D ( $\sim 1350$   $\text{cm}^{-1}$ ) and G ( $\sim 1580$   $\text{cm}^{-1}$ ) bands for graphene present in Fig. 1b [28]. The in-plane  $E_{2g}^1$  mode is associated with opposite vibration of Mo and S atoms while the  $A_{1g}$  mode arises from out-of-plane vibration of two S atoms. The prominent D and G bands corresponding to defect-induced vibration and vibration from  $sp^2$ -bonded carbon atoms suggest RGO nanosheets still have defect-rich edges after hydrothermal reduction [29].

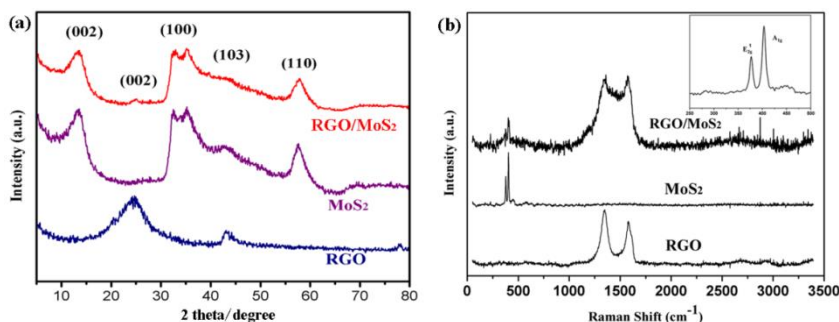


Fig.1. (a) XRD pattern of the RGO/ $\text{MoS}_2$  heterostructure; (b) Raman spectra of RGO,  $\text{MoS}_2$  and RGO/ $\text{MoS}_2$  heterostructures with magnified characteristic Raman signature region.

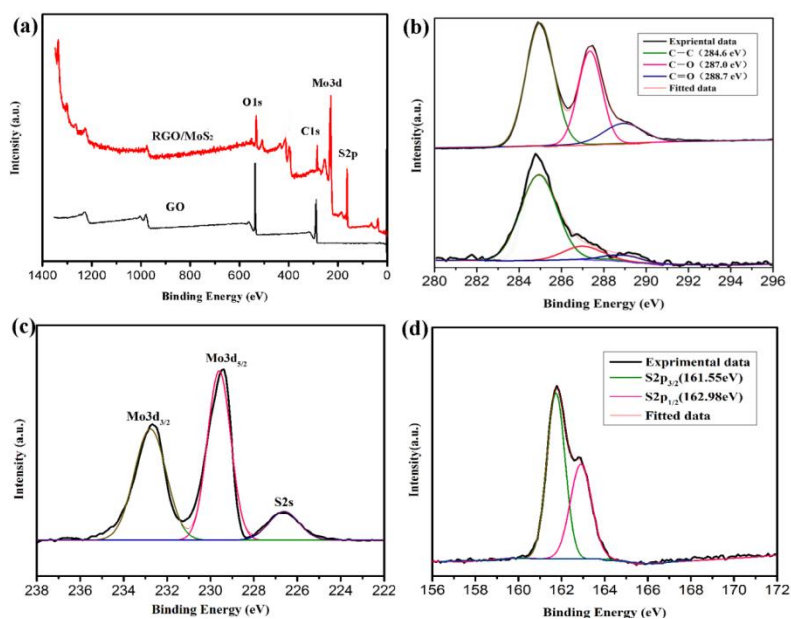


Fig. 2. (a) XPS survey spectra of GO and RGO/MoS<sub>2</sub>; (b) Narrow scan spectra of C1s for GO and RGO/MoS<sub>2</sub>; (c), (d) Narrow scan spectra of Mo3d and S2p for RGO/MoS<sub>2</sub>.

To identify the chemical states of Mo, S, and C elements of the produces, XPS analysis was carried out and shown in Fig. 2. The spectra peaks of RGO/MoS<sub>2</sub> emanating from Mo3d, S2p, C1s and O1s were observed conspicuously at their respective standard values of binding energies (Fig. 2a), which confirmed the existence of these elements in the synthesized produces. Fig. 2b shows XPS fitting of the C1s data for GO and RGO/MoS<sub>2</sub>. Three intense bands located at 284.6 eV, 287.0 eV and 288.7 eV were assigned to the C-C, C-O and C=O, respectively. Contrast with the spectrum of GO, the peak intensities of the C-O and C=O were relatively low among carbon related peaks of RGO/MoS<sub>2</sub>. All of these confirmed the transformation of GO to RGO [30]. The Mo3d XPS spectrum of the MoS<sub>2</sub>/RGO is presented in Fig. 2c, where two main peaks at binding energies of 229.4 and 232.5 eV in Mo3d XPS spectrum should be attributed to Mo3d<sub>3/2</sub> and Mo3d<sub>5/2</sub>, respectively. Fig. 2d shows XPS spectra of the core-level binding energy of S2p RGO/MoS<sub>2</sub>. The doublet peaks with binding energies of 161.55 eV, 162.98 eV for RGO/MoS<sub>2</sub> can be attributed to S2p<sub>3/2</sub> and 2p<sub>1/2</sub> lines, respectively [31].

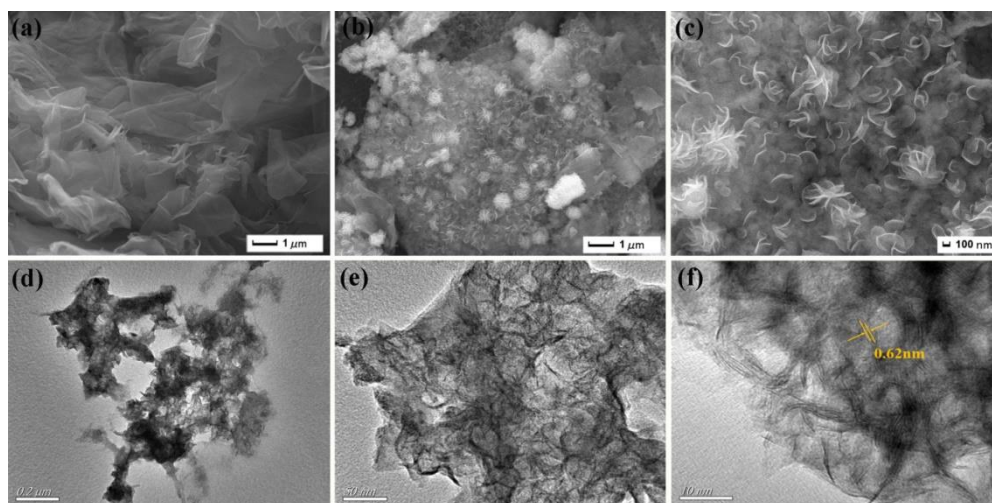


Fig. 3. (a) SEM images of RGO; (b), (c) SEM images of RGO/MoS<sub>2</sub>; (d), (e) TEM image of RGO/MoS<sub>2</sub>; (f) High Resolution TEM images of RGO/MoS<sub>2</sub>

The morphology characterizations of RGO and RGO/MoS<sub>2</sub> are shown in Fig. 3, respectively. RGO which were restored from GO present a typical sheet structure and the surfaces are very smooth (Fig. 3a). It can be found in Fig. 3b that MoS<sub>2</sub> is effective and steady combined with RGO nanosheets, and they were constituted to the 2D heterostructures conjointly. The enlarged image (Fig. 3c) shows that MoS<sub>2</sub> is synthesized with the typical layer structure, which dispersed on RGO nanosheets uniformly. These were endowed with the excellent dispersion effect of RGO nanosheets. As shown in Fig. 3(d, e), the TEM images of RGO/MoS<sub>2</sub> further proved that MoS<sub>2</sub> nanosheets are homogeneously and closely distributed on the surface of RGO nanosheets. High resolution TEM image (Fig. 3f) shows that the interlayer spacing of 0.62 nm measured from lattice fringes can be ascribed to the (002) direction of cubic structured MoS<sub>2</sub>, which is corresponding to the result of XRD.

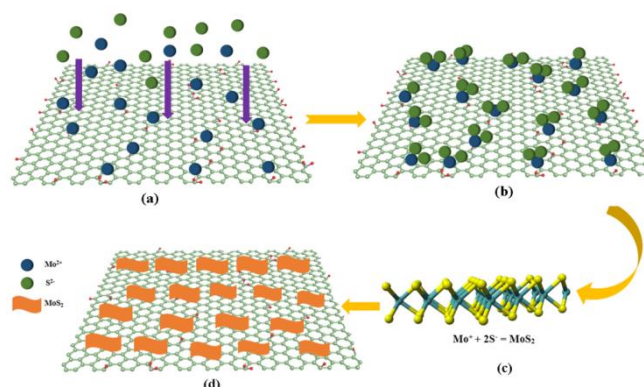


Fig.4. Schematic illustration of synthesise for RGO/MoS<sub>2</sub> heterostructures

Fig. 4 shows schematic illustration of the synthesis of RGO/MoS<sub>2</sub> heterostructures. Originally, numerous carboxylic hydroxyl groups were distributed on the GO sheets with negative charge. The carboxylic and hydroxyl groups were attached on the surface of GO sheets which serve as nucleation site for MoS<sub>2</sub> [32]. In this reaction process, Mo<sup>2+</sup> ions were anchored onto the surface of RGO by the electrostatic interaction or Van der Waals forces of attraction (Fig. 4a). Subsequently, the insertion of thioacetamide provides S<sup>2-</sup> ions to the nucleation site in the reaction mixture (Fig. 4b). Furthermore, as shown in Fig. 4(c, b), these S<sup>2-</sup> ions reacted with Mo<sup>2+</sup> ions to formation the typical MoS<sub>2</sub> sheet structure on the surface of GO. Finally, the carboxylic and hydroxyl groups were reduced gradually and the GO were translated into RGO.

### 3.2. Effect of RGO/MoS<sub>2</sub> heterostructures on vacuum tribological properties

The tribological performances of pure epoxy, RGO and MoS<sub>2</sub> as well as RGO/MoS<sub>2</sub> heterostructures in vacuum environment are investigated. Fig. 5 shows the friction coefficients and wear rate of epoxy, RGO/epoxy, MoS<sub>2</sub>/epoxy and RGO/MoS<sub>2</sub> heterostructures. As shown in Fig. 5a, for single epoxy, the corresponding friction coefficient is the highest with the approximate value of 0.28. With the RGO, MoS<sub>2</sub> and RGO/MoS<sub>2</sub> added to epoxy, the corresponding friction coefficients are reduced obviously. Notably, it could be found from the friction coefficient of MoS<sub>2</sub>/epoxy coating that MoS<sub>2</sub> have the effective friction-reducing ability in vacuum environment, but it shows the obvious instability with the fluctuant trend during the friction process. According to the condition of RGO/MoS<sub>2</sub>/epoxy coating, the friction coefficient is more smoothness with the lower value of 0.05. Further, as shown in Fig. 5b, the wear rate of epoxy shows a big value ( $6.7 \times 10^{-6} \text{ mm}^3 \text{ N}^{-1} \text{ m}^{-1}$ ), indicating the poor anti-wear ability. But the wear rates are declined greatly when RGO, MoS<sub>2</sub> and RGO/MoS<sub>2</sub> were added to epoxy. Moreover, the wear rate of RGO/MoS<sub>2</sub>/epoxy (with the value of  $2.4 \times 10^{-6} \text{ mm}^3 \text{ N}^{-1} \text{ m}^{-1}$ ) is sharply decreases by 50% compared to the wear rate of MoS<sub>2</sub>/epoxy. This could be ascribed to the excellent traction and

support effects of RGO nanosheets. These results proved that RGO/MoS<sub>2</sub> heterostructures possess the best friction-reducing and anti-wear abilities in vacuum environment.

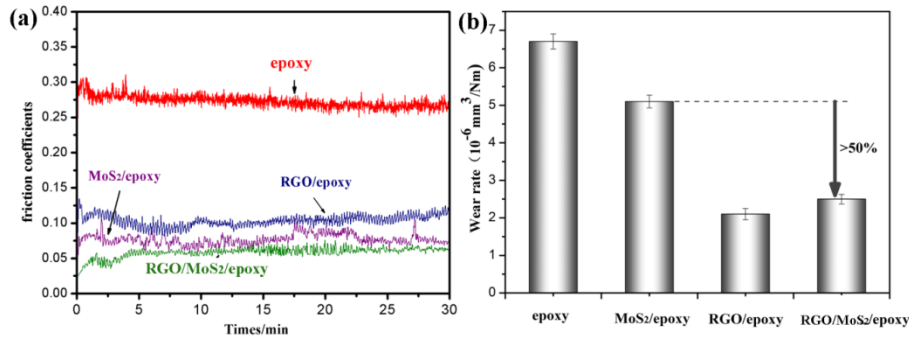


Fig.5. (a) The friction coefficients and (b) wear rates of epoxy, RGO/epoxy, MoS<sub>2</sub>/epoxy and RGO/MoS<sub>2</sub> heterostructures

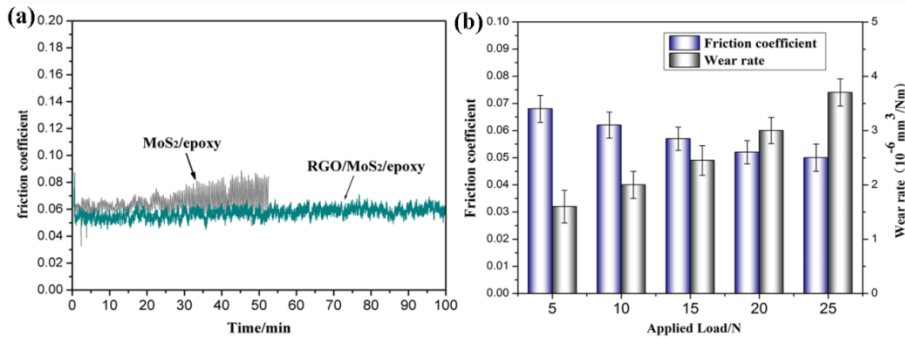


Fig.6. (a) Changes in friction coefficients of MoS<sub>2</sub>/epoxy and RGO/MoS<sub>2</sub>/epoxy coatings until worn out under the load of 10 N; (b) the friction coefficients and wear rates of RGO/MoS<sub>2</sub>/epoxy coatings under the load of 5-25N

Fig. 6 shows the changes in friction coefficients of MoS<sub>2</sub>/epoxy and RGO/MoS<sub>2</sub>/epoxy coatings until worn out and the friction coefficients and wear rates of RGO/MoS<sub>2</sub>/epoxy coatings under the load of 5-25N in vacuum. It can be seen from Fig. 6a that MoS<sub>2</sub>/coating was worn out with a test time of 50 min, and the friction coefficient is presented the big fluctuation after the test time of 30 min. It is quite obvious that RGO/MoS<sub>2</sub>/epoxy coating can work efficiently with a test time of 100 min, and the friction coefficient is very steady. As shown in Fig. 6b, the friction coefficients decrease and the wear rates increase with the applied loads increasingly, but the wear rate is still smallest than MoS<sub>2</sub>. These results further confirmed that RGO/MoS<sub>2</sub> have the best friction-reducing and anti-wear abilities.

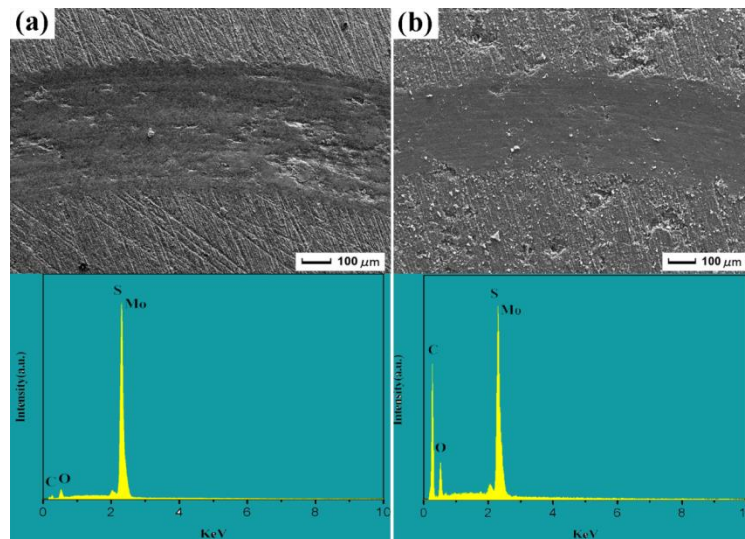


Fig. 7. SEM images of the worn surfaces of (a) MoS<sub>2</sub>/epoxy and (b) RGO/MoS<sub>2</sub>/epoxy coatings

To study the details of MoS<sub>2</sub>/epoxy and RGO/MoS<sub>2</sub>/epoxy coatings, SEM images of the worn surfaces are shown in Fig. 7. Obviously, the worn surface of MoS<sub>2</sub>/epoxy (Fig. 7a) is very rough with numerous corrosion pits, which are formed due to the damage of MoS<sub>2</sub> during the wear process. Particularly, it could be found in Fig. 7b that the worn surface of RGO/MoS<sub>2</sub>/epoxy coating is very smooth and the width is decreased markedly, meanwhile, the corrosion pits are disappeared by compare to MoS<sub>2</sub>/epoxy. Furthermore, the noncontact three-dimensional cross-section images of wear tracks obtained on surface of MoS<sub>2</sub>/epoxy and RGO/MoS<sub>2</sub>/epoxy coatings are shown in Fig. 8. The widths of worn surface for MoS<sub>2</sub>/epoxy and RGO/MoS<sub>2</sub>/epoxy coatings are 472 μm and 363 μm, and the depths are 9.5 μm and 4.1 μm, respectively. The obvious reductions of the width and depth have a similar trend with the friction coefficient and wear rate. The results forceful proved that RGO/MoS<sub>2</sub> have the wonderful friction-reducing and anti-wear abilities.

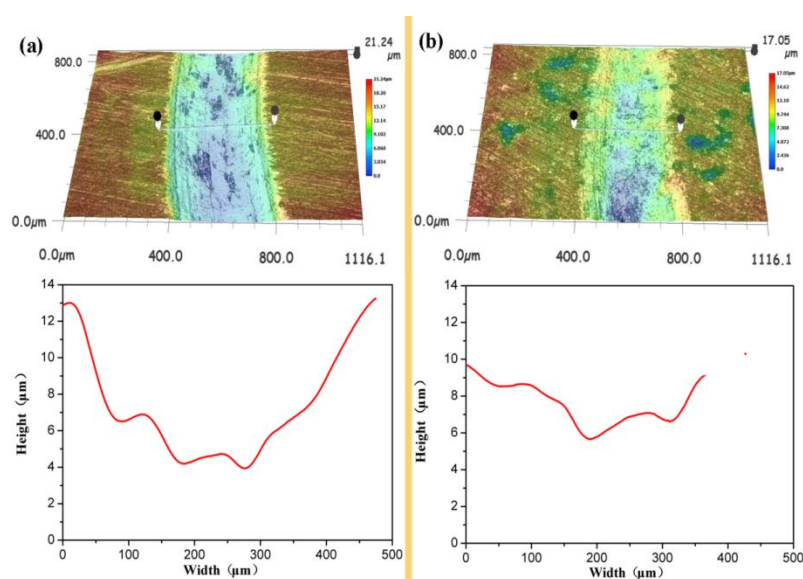


Fig. 8. Noncontact three-dimensional cross-section images of wear tracks obtained on surface of MoS<sub>2</sub>/epoxy and RGO/MoS<sub>2</sub>/epoxy coatings

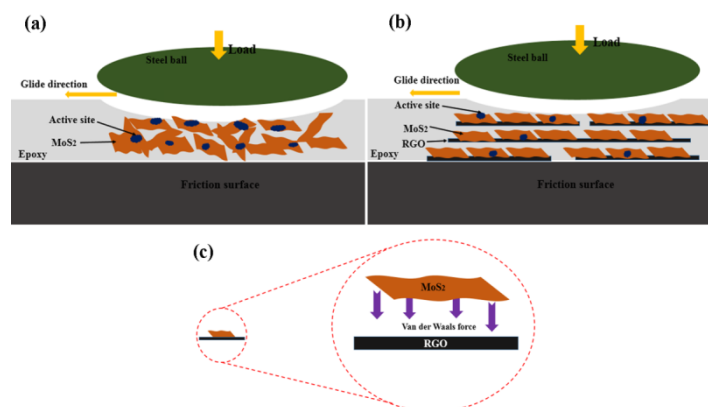


Fig. 9. The tribological mechanisms of (a) MoS<sub>2</sub> nanosheets and (b) RGO/MoS<sub>2</sub> heterostructures

In order to describe the traction and support effects of RGO nanosheets for MoS<sub>2</sub>, the tribological mechanism diagrams of MoS<sub>2</sub> nanosheets and RGO/MoS<sub>2</sub> heterostructures are shown in Fig. 9. When MoS<sub>2</sub> nanosheets were added into epoxy, they tend to conglutinate and stack together due to poor dispersive capacity (Fig. 9a). In wear test, there was no other atoms to terminate the dangling bonds and result in generate the active sites, which further lead to MoS<sub>2</sub> molecules were adhered between each other. Therefore, single MoS<sub>2</sub> nanosheets have low anti-wear ability, and they were tended to damage under the applied load [33]. When MoS<sub>2</sub> nanosheets were assembled on the RGO nanosheets, MoS<sub>2</sub> nanosheets were dispersed equably, and MoS<sub>2</sub> nanosheets were sheared by only the shear force under the control of traction and support effects of RGO nanosheets (Fig. 9b). The dangling bonds and active sites were restricted by the Van der Waals force between MoS<sub>2</sub> and RGO (Fig. 9c). All of these factors would protect MoS<sub>2</sub> not to destroy, so the RGO/MoS<sub>2</sub> heterostructures were endowed with the excellent friction-reducing and anti-wear abilities.

#### 4. Conclusions

RGO/MoS<sub>2</sub> heterostructures were fabricated via a facile hydrothermal method. Varieties of physical characterizations are employed to confirm the well-controlled form of MoS<sub>2</sub> and investigate the structural quality of RGO/MoS<sub>2</sub> heterostructures. Due to the unique traction and support effects of RGO nanosheets, the as-prepared RGO/MoS<sub>2</sub> sample presents the improved dispersibility and stability. Tribological investigations of RGO/MoS<sub>2</sub> heterostructures were carried out under vacuum environment. The results indicated that RGO/MoS<sub>2</sub> heterostructures have the excellent friction-reducing and anti-wear abilities, and these abilities are enhanced greatly by compare to single MoS<sub>2</sub>.

The efficient friction-reducing and anti-wear abilities of RGO/MoS<sub>2</sub> heterostructures are attributed to the excellent traction and support effects of RGO, meanwhile, RGO nanosheets can terminate the dangling bonds and reduce the active sites of MoS<sub>2</sub>. Furthermore, this work highlights a pathway to expand potential applications of RGO/MoS<sub>2</sub> heterostructures in space tribological field and the assistance ability of RGO nanosheets.

#### Acknowledgments

This work was supported by the Natural Science Foundation of Jiangsu Province, China (BK20140562).

## References

- [1] G. Colas, A. Saulot, C. Godeau, Y. Michel, Y. Berthier, *Wear*. **305**, 193 (2013).
- [2] G. Theiler, T. Gradt, *Wear*. **269**, 280 (2010).
- [3] X. Quan, M. Hu, X.M. Gao, Y.L. Fu, L.J. Weng, D.S. Wang, D. Jian, J.Y. Sun, *Tribol. Int.* **99**, 59 (2016).
- [4] T.Z. Zou, J.P. Tu, S.C. Zhang, L.M. Chen, Q. Wang, L.L. Zhang, D.N. He, *Mater. Sci. Eng.A.* **426**, 164 (2006).
- [5] L. Liu, Z.B. Huang, P. Huang, *Tribol. Int.* **104**, 305 (2016).
- [6] Y. Ding, Y.F. Zhou, W.Y. Nie, P.P. Chen, *Appl. Surf. Sci.* **357**, 1608 (2015).
- [7] J. Cheng, J.M. Zhen, S.Y. Zhu, J. Yang, J.Q. Ma, W.S. Li, W.M. Liu, *Mater. Des.* **122**, 207 (2017).
- [8] F.S. Liu, Y.Z. Zhou, D.C. Liu, X.M. Chen, C.F. Yang, L. Zhou, *Vacuum*. **139**, 145 (2017).
- [9] I. Efeoglu, Ö Baran, F. Yetim, S. Altıntaş, *Surf. Coat. Tech.* **203**, 768 (2008).
- [10] X.Z. Ding, X.T. Zeng, X.Y. He, Z. Chen, *Surf. Coat. Tech.* **205**, 226 (2010).
- [11] X.J. Zheng, Y.F. Xu, J. Geng, Y.B. Peng, D. Olson, X.G. Hu, *Tribol. Int.* **102**, 81 (2016).
- [12] P. Devi, P. Kumar, C. Sharma, C. Sharma, Mahesh Kumar, M. Nayak, *Mater. Lett.* **181**, 100 (2016).
- [13] J. Zhou, H. Xiao, B. Zhou, F.F. Huang, S.B. Zhou, W. Xiao, D.H. Wang, *Appl. Surf. Sci.* **358**, 154 (2015).
- [14] A. A Jeffery, S. R. Rao, M. Rajamathi, *Carbon*. **112**, 10 (2017).
- [15] D. Berman, A. Erdemir, A.V. Sumant, *Carbon*. **59**, 169 (2013).
- [16] J. Llorente, B. Román-Manso, P. Miranzo, M. Belmonte, *J. Eur. Cerma. Soc.* **36**, 431 (2016).
- [17] A. M. Golsheikh, N.M. Huang, H.N. Lim, C.H. Chia, I. Harrison, M.R. Muhamad, *Chem. Eng. J.* **218**, 278 (2013).
- [18] S. Stankovich, D.A. Dikin, G. H. B. Dommett, K. M. Kohlhaas, E. J. Zimney, *Nature*. **442**, 20 (2006).
- [19] S.R. Shin, Y.C. Li, H.L. Jang, P. Khoshakhlagh, M. Akbari, A. Nasajpour, *Adv. Drug. Deliver. Rev.* **105**, 257 (2016).
- [20] S. Watanabe, J. Noshiro, S. Miyake, *Surf. Coat. Tech.* **188-189**, 645 (2004).
- [21] Z.L. Cheng, W. Li, Z. Liu, *J. Alloy. Compd.* **705**, 386 (2017).
- [22] N.T. Shelke, B.R. Karche, *J. Alloy. Compd.* **653**, 300 (2013).
- [23] K.L. Gong, X.H. Wu, G.Q. Zhao, X.B. Wang, *Tribol. Int.* **110**, 2 (2017).
- [24] Z.Y. Chen, H.X. Yan, T.Y. Liu, *S. Compos. Sci. Technol.* **125**, 49 (2016).
- [25] M.S. Zhang, B.B. Chen, H. Tang, G.G. Tang, C.S. Li, *RSC Adv*, **5**, 1419 (2015).
- [26] J.S. Chen, J. Yang, B.B. Chen, S. Liu, C.S. Li, *Surf. Coat. Tech.* **305**, 25 (2016).
- [27] K.M. Hou, J.Q. Wang, Z.G. Yang, L.M. Ma, S.R. Yang, *Carbon*. **115**, 85 (2017).
- [28] K. Zhang, M.S. Song, J. H. Park, J.T. Lee, J.M. Choi, *Inorg. Chem.* **52**, 9809 (2013).
- [29] X.M. Geng, W. Wu, N. Li, W.W. Sun, J. Armstrong, A. Al-hilo, *Adv. Funct. Mater.* **24**, 6125 (2014).
- [30] H. Borchert, St. Haubold, M. Haase, H. Weller, *Nano. Lett.* **2**, 151 (2002).
- [31] L.W. Xing, Z. F. Ma, *Microchim Acta.* **183**, 259 (2016).
- [32] S. Jindal, S.M. Giripunje, *Superlattice. Microst.* **1**, 11 (2016).
- [33] P. E. Hovsepian, P. Mandal, A.P. Ehiasarian, G. Sáfrán, *Appl. Surf. Sci.* **366**, 262 (2016).